Cell Mechanics Modeling and Identification by Atomic Force Microscopy

Michael R. P. Ragazzon * **Marialena Vagia** **
J. Tommy Gravdahl *

* *Department of Engineering Cybernetics, NTNU, Norwegian University of Science and Technology, Trondheim, Norway (e-mail: {ragazzon, Tommy.Gravdahl}@itk.ntnu.no).*
** *SINTEF ICT, Applied Cybernetics (e-mail: Marialena.Vagia@sintef.no).*

Abstract: Cells are complex living organisms often described as the building blocks of life. The mechanical properties of such cells have been shown to be effective for medical diagnosis. Previous research in this area focus primarily on static methods by identifying local variations in cell elasticity. Atomic force microscopy (AFM) has shown to be effective for such measurements. In this paper we extend on this methodology by developing a dynamic viscoelastic model of the cell, constructed to be well suited for parameter identification. A parameter estimator is then designed for identifying the spatially resolved mechanical properties of the cell. The parameter estimates are shown to converge exponentially fast to the real parameters by employing the provided control input. A key property of this online estimation scheme is allowing for mechanical changes in the cell to be detected over time. Furthermore, the approach can be applied to the problem of identifying the mechanical properties of any elastic material that can be scanned in AFM. A simulation study shows the effectiveness of the methodology.

Keywords: Mechanical properties; Parameter identification; Biomedical systems; Dynamic models; Positioning systems

1. INTRODUCTION

Biological cell samples can interact with the external environment by generating forces originating from their mechanical properties. Such mechanical properties are frequently linked to fundamental processes including cell division, locomotion and invasion, differentiation, mechanotransduction, and apoptosis (Reichl et al., 2005; Kumar and Weaver, 2009). It has also been implicated that a change in the cell elasticity is noticed in the pathogenesis of many progressive diseases including cancer (Parsons et al., 2010) and cardiovascular diseases (Bao and Suresh, 2003), diabetic complications, vascular diseases, kidney diseases, Alzheimer's and malaria. Among the above mentioned diseases, and many more that can be described by the same properties, carcinomas attracts the main interest of the scientific community. A large effort has been devoted to their diagnosis and treatment, and any possible research in new diagnostic methods that could lead to earlier and more accurate diagnosis attracts a huge interest in the scientific community (Lekka et al., 2012b).

In practice, there is no need to highlight the importance of studying the properties of carcinoid cells (Sokolov, 2007). The current cancer diagnosis relies mostly on morphological examination of exfoliated and aspirated cells or surgically removed tissue. Up to now, as far as the standard diagnosis is concerned this classical approach seems to be satisfactory (Lekka et al., 2012a; Ramis-Conde et al., 2008). However, new tools are needed in order to offer the patients an earlier diagnosis which has been shown to be one of the most important factors in the prognostic outcome.

In order for new diagnosis tools to become available, it is important to gain a detailed knowledge of the mechanical properties of live cells that are to be examined. Different techniques have been proposed so far, including methods like micro-pipette manipulation (Discher et al., 2008), magnetic bead twisting (Bausch et al., 1998), and optical tweezers (Guck et al., 2002). With these techniques, local variations in the viscoelastic power law parameters have been observed (Hecht et al., 2015).

Aside of the above mentioned ones, there is another technique gaining more and more focus in the recent years which utilize atomic force microscopy (AFM) (Weisenhorn et al., 1993; Degertekin et al., 2001). AFM is one of the major techniques responsible for the emergence of modern nanotechnology. AFM works by having a tip located at the end of a microcantilever. The cantilever can be controlled in the vertical direction. As the cantilever is lowered and the tip touches the sample, the cantilever will start deflecting. This deflection can be measured. By keeping the deflection constant in a feedback loop controlling the cantilever position, the topography of the sample can be recorded as the sample is moved in the lateral directions.

There are several variations to the control mechanism in AFM, including dynamic modes (Garcia and Perez, 2002) such as amplitude modulated control where the cantilever is oscillated and the amplitude is estimated (Ragazzon

et al., 2016) and used as the feedback signal. Other methods use a tip-sample force estimate directly as the feedback signal (Jeong et al., 2006; Karvinen et al., 2014), or invert the force to estimate the tip-sample distance itself (Ragazzon et al., 2015).

AFM has a number of features that makes it extremely valuable in biology (Sokolov, 2007). The main beneficial feature is its ability to study biological objects directly in their natural conditions (Benitez and Toca-Herrera, 2014). In addition, it has the major feature of using the AFM probe to indent a cell to study cell mechanics by recording the cantilever deflection while deforming the cell (Guz et al., 2014). Such approaches are often based on Hertz or Sneddon model of contact mechanics to find measurements of elasticity, experiments for which are usually performed statically (Sokolov et al., 2013).

The amplitude and phase-shift in dynamic modes of AFM have been shown to be correlated to the viscoelastic properties of the sample (Radmacher et al., 1993; Cartagena-Rivera et al., 2015). Multiple harmonics can also be utilized for mapping such properties in dynamic mode (Raman et al., 2011). These approaches relate the cantilever indentation into the surface to local elastic and viscous properties. In this paper however, we take a unique approach for extracting similar properties from a sample.

In this paper we propose to model the sample as a dynamic model with unknown parameters. By employing identification techniques from the control literature, we allow these parameters to be estimated directly and thereby making it possible to observe changes over time. There is no need for post-processing of the data or to explicitly find a mapping from the deflection data to the viscoelastic parameters as used in previous approaches. The estimated parameters are guaranteed to converge to the real values exponentially fast provided a suitable control input is chosen.

Additionally, this approach is easily extendable for future work as the sample model can be modified to fit observational data. This allows possibly including phenomena such as creep, hysteresis, plasticity, and nonlinear elastic and damping effects. However, in this paper we restrict ourselves to observing elastic (spring constants), and viscous (damping constants) properties of the sample, as well as topography. This is not a complete description of the mechanics of the cell. However, since these properties have already been shown to be effective in applications such as medical diagnosis, it is proposed as a good starting point.

2. CANTILEVER-SAMPLE SYSTEM MODELING

The purpose of the system modeling is to provide a dynamic model description of a cantilever interacting with a general viscoelastic sample material, while allowing for simple identification of the model parameters by use of atomic force microscopy. Additionally, the presented model can easily be extended and modified to suit the characteristics of various materials.

The sample to be measured is modeled by lumped spring-damper elements along the lateral xy-axes as illustrated in Figure 1. The elements can be compressed in the vertical z-direction. An attractive feature of this model is that it allows for capturing spatial variations in stiffness and damping properties. Moreover, the fidelity of the model can be chosen to fit the task at hand, by selecting an appropriate number of spring-damper elements. The only measurable signal is the cantilever deflection D commonly measured by a photo-detector setup as illustrated in Figure 2. The cantilever base position U can be controlled for movement in the vertical direction. The vertical position of the cantilever tip is given by Z with the relationship

$$Z = U - D. \tag{1}$$

Additionally, the tip can be controlled in the xy-direction (Eielsen et al., 2013). The resulting position of the center of the tip is given by (X, Y, Z) in the coordinate system (x, y, z) seen in Figure 1.

The cantilever-sample dynamics can be described by three main components as seen in Figure 3. The cantilever dynamics is subjected to external sample force which generates a deflection along the vertical axis. The tip geometry and position is then used to determine the (possibly compressed) positions of each sample spring-damper element. The compressed elements in turn creates a restoration force acting on the cantilever tip. The details of each of these components will be described in the following.

2.1 Cantilever Dynamics

The cantilever dynamics can be approximated by its first resonance mode, resulting in the spring-damper system

$$M\ddot{Z} = KD + C\dot{D} + F_{\text{sample}} \tag{2}$$

$$= K(U - Z) + C(\dot{U} - \dot{Z}) + F_{\text{sample}} \tag{3}$$

where M is the effective mass of the cantilever (Bhushan and Marti, 2010), K, C are the cantilever spring and damping constants respectively, and F_{sample} is the force from the sample acting on the cantilever tip.

2.2 Tip Geometry

In addition to a description of the tip geometry, the position of the cantilever tip can now be used to determine the deflection and motion of each individual spring element in the sample.

In this paper the tip is modeled by a spherical shape with radius R. A dull spherical probe is generally advantageous when scanning soft materials such as cells (Sokolov et al., 2013). However, this choice can easily be extended for additional geometrical shapes.

A spherical shape leads to the following relationship between the tip and the ith sample element's position z_i and velocity $\dot{z}_i$,

$$z_i = Z - \sqrt{R^2 - (X - x_i)^2 - (Y - y_i)^2} \tag{4}$$

$$\dot{z}_i = \dot{Z} \tag{5}$$

where (x_i, y_i) is the lateral position of the ith sample element. It has been used that $\dot{X}, \dot{Y}$ are assumed to be zero while the tip is in contact with the sample.

2.3 Sample Force

The ith spring-damper element in the sample has a rest-position z_i^0 which represents the sample topography at

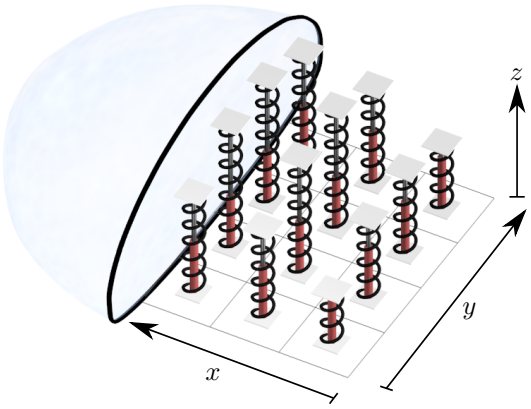

Fig. 1. Biological cell modeled by spring-damper elements.

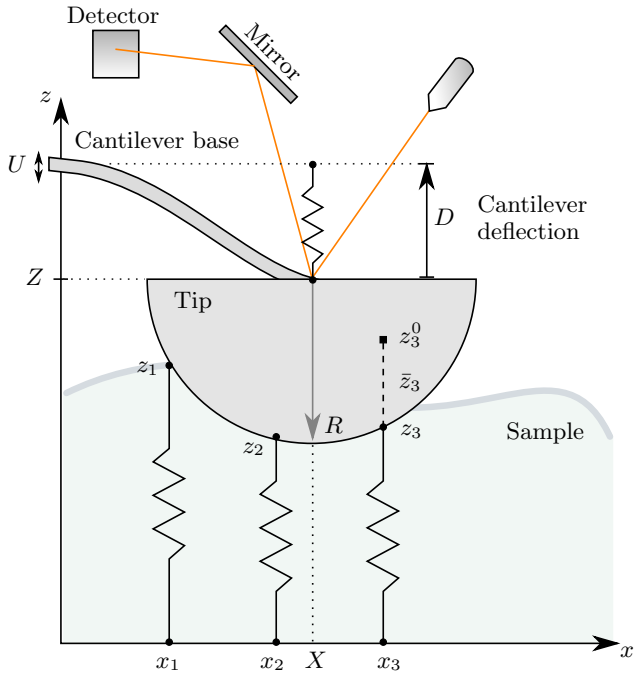

Fig. 2. Cantilever-cell system modeling.

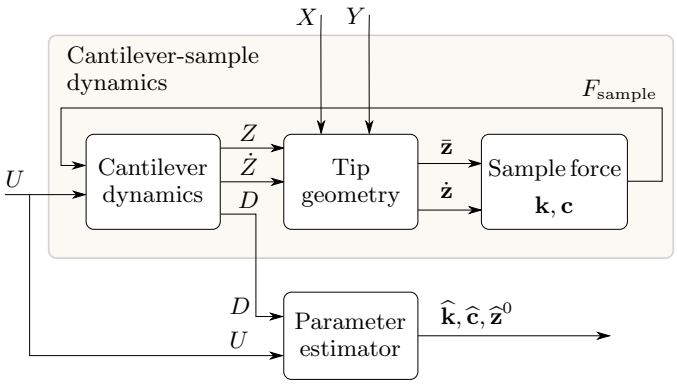

Fig. 3. Block diagram of the cantilever-sample dynamics and parameter estimator. The parameter estimates are based solely on measurements of the deflection output D and the vertical position control input U.

the given lateral position (x_i, y_i). When the cantilever tip presses onto the sample the element will be compressed to a new position z_i provided in the previous section. This generates a restoration force according to Hooke's law

$$F_{ki} = k_i \bar{z}_i \tag{6}$$

where k_i is the spring constant and

$$\bar{z}_i \triangleq z_i - z_i^0 \tag{7}$$

is the deflection of the ith sample element, or equivalently the indentation of the tip into the element. Additionally, a damping force is added according to

$$F_{ci} = c_i \dot{z}_i \tag{8}$$

where c_i is the damping parameter. Note that other, possibly nonlinear, models of springs and dampers can be employed in order to capture more complex behavior.

The total force acting from the sample on the tip is given by

$$F_{\text{sample}} = \sum_{i \in \mathcal{W}} F_{ki} + F_{ci}. \tag{9}$$

where $\mathcal{W} = \mathcal{W}(X, Y, Z)$ is the active set of sample elements the tip is in contact with, that is

$$\mathcal{W} = \left\{ i : \bar{z}_i < 0 \wedge (X - x_i)^2 + (Y - y_i)^2 < R^2 \right\}. \tag{10}$$

The springs are thus modeled to solely provide repulsive forces against tip. A more detailed model could allow for attractive spring forces as the tip approaches the sample, although this is outside the scope of this paper.

In the following, the vectors $\mathbf{k}, \mathbf{c}, \mathbf{z}^0$ are used to refer to the family of elements, e.g. $\mathbf{k} = \{k_1, ..., k_n\}$ where n is the number of spring-damper elements in the sample.

3. PARAMETER IDENTIFICATION

The modeled tip-sample system was described in the previous section. The goal of this section is to show how the unknown parameters of the system, $\mathbf{k}, \mathbf{c}, \mathbf{z}^0$, can be estimated. As seen in Figure 3 the parameter estimator is separated from the system and only the cantilever deflection D and vertical control input signal U is assumed available for measurement.

An online identification scheme will be developed for this purpose. Having an online scheme allows us both to view the estimates as the cantilever scans the surface. Additionally, this allows us to view live changes in the sample being scanned.

The strategy for identifying the topography and unknown parameters involves tapping into every region of the sample. The cantilever tip is moved in a raster pattern over the sample. At periodic intervals the lateral movement is paused and the tip is lowered into the sample, a proper excitation signal is applied on the input until the parameter estimates converge, before the tip is raised and the tapping operation repeats at the next position.

At first the system equations will be written in a form suitable for parameter identification, before the estimator is presented.

3.1 System Equations

The Laplace-domain description of the cantilever-sample dynamics can be found using (3)–(10), which gives

$$\left(Ms^2+Cs+K\right)D+\sum_{i\in\mathcal{W}}\left(c_is+k_i\right)\bar{z}_i=(Cs+K)U. \quad (11)$$

The set $\mathcal{W}$ is dependent on the tip position, and thus unique for each tap. By tapping into every region of the sample, the unknown parameters c_i, k_i will contribute to the known signals D, U and can in principle be discovered. In addition to c_i, k_i being unknown, $\bar{z}_i$ is also unknown because of the dependency on the topography term, $\bar{z}_i = z_i - z_i^0$. The topography term could be added to the parameter estimator scheme, but we will treat it separately and assume $\bar{z}_i$ as known for now. Identification of the topography will be discussed later.

Since the unknown terms in (11) appear linearly in the signals, this is in principle a simple estimation task. However, we have $2\left|\mathcal{W}\right|$ number of elements to estimate, that is, one c_i, k_i for each element in the active set $\mathcal{W}$. This can be very demanding in terms of parameter convergence and requires a carefully designed input signal to make it persistently exciting. Additionally, it may require that each $\bar{z}_i$ is unique, that is, the topography must be unique at each point $i \in \mathcal{W}$ for the parameters to converge.

To reduce the number of parameters to be estimated simultaneously we approximate (11) by the estimation model valid during a single tap,

$$\left(Ms^2+Cs+K\right)D+(cs+k)\bar{z}=(Cs+K)U \quad (12)$$

where c, k approximates the sum of $c_i, k_i \in \mathcal{W}$ and $\bar{z}$ approximates an average of $\bar{z}_i \in \mathcal{W}$. Thus, c, k and z^0 in $\bar{z}$ are possibly unique at each tap position, but constant during a single tap. By allowing the parameter estimator to identify the parameters during each tap $j \in \{1, ..., m\}$ where m is the total number of taps for the complete scan, local variations in these parameters can be stored, referred to as c_j, k_j, z_j^0. This model simplification gives the parameter estimator two unknown parameters to estimate during each tap (assuming z_j^0 known for now), and effectively reduces the spatial resolution of the identified parameters at the benefit of possibly faster convergence time and lower demand for complexity in the input signal design.

In reality the parameters will vary continuously over the sample. Thus, discretizing the plant model more finely than the parameter identification model makes sense from a physical point of view. The estimated values of c, k, z^0 from the parameter estimator are hereby referred to as $\hat{c}, \hat{k}, \hat{z}^0$. The vectors $\widehat{\mathbf{k}}, \widehat{\mathbf{c}}, \widehat{\mathbf{z}}^0$ are used to refer to the family of identified parameters, such that $\widehat{\mathbf{k}} = \{\hat{k}_1, ..., \hat{k}_m\}$.

3.2 Parametric System Model

We want our system on a linear-in-the-parameters form

$$w = \boldsymbol{\theta}^T\boldsymbol{\phi} \quad (13)$$

where w is the signal scalar, $\boldsymbol{\theta} = [c, k]^T$ is the parameter vector, and $\boldsymbol{\phi}$ is the signal vector. This form is suitable for implementation of various estimation techniques as presented in Ioannou and Sun (1996). Rearranging (12) we get

$$(Cs+K)U-\left(Ms^2+Cs+K\right)D=(cs+k)\,\bar{z} \quad (14)$$

$$w' = cs\bar{z}+k\bar{z} \quad (15)$$

$$= [c, k][s\bar{z}, \bar{z}]^T \quad (16)$$

where w' is defined by the left hand side of (14). As s^2 appears directly in w', we filter each side by a stable filter of relative degree 2. This makes all signals proper and avoids pure differentiation. The filter $1/\Lambda(s) = 1/(1+\tau s)^2$ is chosen where τ is a tunable positive constant, this gives

$$\frac{w'}{\Lambda(s)} = [c, k]\left[\frac{s\bar{z}}{\Lambda(s)}, \frac{\bar{z}}{\Lambda(s)}\right]^T \quad (17)$$

The system is now on the form (13) with

$$w = \tfrac{1}{\Lambda(s)}\left((Cs+K)u-\left(Ms^2+Cs+K\right)d\right) \quad (18)$$

$$\boldsymbol{\phi} = \left[\frac{s\bar{z}}{\Lambda(s)}, \frac{\bar{z}}{\Lambda(s)}\right]^T \quad (19)$$

$$\boldsymbol{\theta} = [c, k]^T \quad (20)$$

3.3 Parameter Estimator

The system (13),(18)-(20) is now suitable for implementation of a variety of estimation methods given in e.g. Ioannou and Sun (1996). A least squares method with forgetting factor was chosen for implementation. The forgetting factor is useful as the parameters are assumed to be non-homogeneous between each tap. The method is restated here for convenience to the reader:

$$\widehat{w} = \widehat{\boldsymbol{\theta}}^T\boldsymbol{\phi} \quad (21)$$

$$\varepsilon = (w-\widehat{w})/m^2 \quad (22)$$

$$m^2 = 1+\alpha\boldsymbol{\phi}^T\boldsymbol{\phi} \quad (23)$$

$$\dot{\widehat{\boldsymbol{\theta}}} = \mathbf{P}\varepsilon\boldsymbol{\phi} \quad (24)$$

$$\dot{\mathbf{P}} = \begin{cases}\beta\mathbf{P}-\mathbf{P}\frac{\boldsymbol{\phi}\boldsymbol{\phi}^T}{m^2}\mathbf{P}, & \text{if } \|\mathbf{P}\| \le R_0\\ 0, & \text{otherwise}\end{cases} \quad (25)$$

$$\mathbf{P}(0) = \mathbf{P}_0 \quad (26)$$

where $\widehat{\boldsymbol{\theta}} = [\hat{c}, \hat{k}]^T$ is the parameter estimate vector, α, β, R_0 are positive constants, and $\mathbf{P} \in \mathbb{R}^{2\times 2}$ is the covariance matrix. The method guarantees stability of ε and boundedness of $\widehat{\boldsymbol{\theta}}$. Exponential convergence of $\widehat{\boldsymbol{\theta}}$ to $\boldsymbol{\theta}$ is guaranteed as long as the signal vector $\boldsymbol{\phi}$ is persistently exciting (PE). For more details and proofs, see Ioannou and Sun (1996).

The next theorem gives conditions for $\boldsymbol{\phi}$ being PE, and the exponential convergence properties of the parameter estimates $\widehat{\boldsymbol{\theta}}$.

Theorem 1. (Persistency of excitation). Apply the cantilever input signal $U = u_0 + a\sin(\omega_0 t)$ for any positive constants a, ω_0, and let the constant u_0 be small enough such that the cantilever tip is in contact with the surface, i.e. $\bar{z} < 0, \forall\, t$. Then $\boldsymbol{\phi}$ is persistently exciting (PE) and $\widehat{\boldsymbol{\theta}} \to \boldsymbol{\theta}$ exponentially fast.

Proof. Expand the signal vector $\boldsymbol{\phi}$ such that

$$\boldsymbol{\phi} = \mathbf{H}(s)\bar{z}, \quad \mathbf{H}(s) = \begin{bmatrix}\frac{s}{(1+\tau s)^2}\\ \frac{1}{(1+\tau s)^2}\end{bmatrix}$$

Define the matrix $\mathbf{A}$ such that

$$\mathbf{A}(j\omega_1, j\omega_2) \triangleq [\,\mathbf{H}(j\omega_1)\ \mathbf{H}(j\omega_2)\,] = \begin{bmatrix}\frac{j\omega_1}{(1+\tau j\omega_1)^2} & \frac{j\omega_2}{(1+\tau j\omega_2)^2}\\ \frac{1}{(1+\tau j\omega_1)^2} & \frac{1}{(1+\tau j\omega_2)^2}\end{bmatrix}$$

Taking the determinant of $\mathbf{A}$ gives

$$|\mathbf{A}(j\omega_1, j\omega_2)| = \frac{1}{(1+\tau j\omega_1)^2(1+\tau j\omega_2)^2}(j\omega_1 - j\omega_2)$$
$$\neq 0 \,\forall\, \{\omega_1, \omega_2 \in \mathbb{R} \,:\, \omega_1 \neq \omega_2\}$$

Thus $\mathbf{H}(j\omega_1), \mathbf{H}(j\omega_2)$ are linearly independent on $\mathbb{C}^2$ $\forall\, \{\omega_1, \omega_2 \in \mathbb{R} \,:\, \omega_1 \neq \omega_2\}$. By Theorem 5.2.1 in Ioannou and Sun (1996) $\boldsymbol{\phi}$ is then PE if and only if $\bar{z}$ is sufficiently rich of order 2.

By Definition 5.2.1 in Ioannou and Sun (1996) the signal $U = u_0 + a\sin(\omega_0 t)$ is sufficiently rich of order 2. The transformation from U to $\bar{z}$ is seen to be linear and stable considering (11) and the equations of Section 2, which means that a sinusoidal input on U results in a sinusoidal output on $\bar{z}$ with amplitude $\left|\frac{\bar{z}}{U}(j\omega_0)\right|$, phase $\angle\frac{\bar{z}}{U}(j\omega_0)$ and frequency ω_0. The signal $\bar{z}$ is thus sufficiently rich of order 2. Thus, $\boldsymbol{\phi}$ is PE. Additionally, $\boldsymbol{\phi}$ is bounded since $\dot{U}$ is bounded and $\mathbf{H}(s), \frac{\bar{z}}{U}(s)$ are stable. Then, by Corollary 4.3.1 in Ioannou and Sun (1996) the parameter vector $\widehat{\boldsymbol{\theta}} \to \boldsymbol{\theta}$ exponentially fast. □

3.4 Estimation of indentation depth and topography

Finally, the signal $\bar{z}$ describing the indentation depth of the cantilever tip into the sample during a tap needs to be generated. As the tip enters the sample the cantilever will start to deflect. This point is recorded and used as the topography estimate $\hat{z}^0$ at the current tip position, and the indentation depth estimate $\hat{\bar{z}}$ is then given by

$$\hat{\bar{z}}(t) = Z(t) - \hat{z}^0. \tag{27}$$

The topography estimate $\hat{z}^0$ is stored after each tap j generating the estimate of the complete sample topography $\hat{z}^0_j \,\forall\, j$. Additionally, a low-pass filter G_{lp} for attenuation of measurement noise and a hysteresis loop for avoiding retriggering during sample penetration is used in the implementation. The procedure is summarized as follows:

- Record the time $t_1 = t$ at rising edge of the boolean signal $G_{lp}D < -\delta$, for some positive constant δ.
- Create a hysteresis loop for t_1 by disabling retriggering until $G_{lp}D < -\delta_+$ where $\delta_+ > \delta$.
- Then $\hat{z}^0 = Z(t_1)$ and $\hat{\bar{z}}(t) = Z(t) - \hat{z}^0$, where as previously $Z(t) = U(t) - D(t)$.
- Store $\hat{z}^0_j = \hat{z}^0$ for the current tap j.

4. SIMULATION RESULTS

The tip-sample system as well as the parameter system as described in the previous sections have been implemented for simulations following the setup in Figure 3. The objective of the simulations is to identify the parameters of the mechanical model of the cell, $\mathbf{c}, \mathbf{k}, \mathbf{z}^0$, using this setup. The parameters were generated by using Gaussian filters on normally distributed random numbers and weighted by a spherical function to resemble a cell. The scanning area was chosen to be $1 \times 1\,\mu\text{m}$ discretized into 32 elements along each axis. The simulation was setup to perform 10 taps along each axis for a total of 100 taps. This results in a 10×10 spatial resolution for each parameter to be identified $\widehat{\mathbf{k}}, \widehat{\mathbf{c}}, \widehat{\mathbf{z}}^0$.

The generated parameters are plotted against the identified parameters and mapped to the spatial dimensions in Figure 4–6 for $\mathbf{c}, \mathbf{k}, \mathbf{z}^0$ respectively. The parameters along a cross section of the map is plotted in Figure 7.

The exponential convergence properties of the parameter estimator is demonstrated in Figure 8, where the estimates of k, c are plotted against time during two taps. Additionally, the input signal is plotted showing how the cantilever is lowered into the sample and then starts oscillating to ensure persistency of excitation during identification. Although a single sinusoidal signal is necessary for PE, we use two sinusoids for faster convergence.

Measurement noise has been added to the deflection output by Gaussian distributed white noise with standard deviation 1 nm. The values of $\widehat{\boldsymbol{c}}, \widehat{\boldsymbol{k}}$ are scaled in the plots by a constant $\sim 1/|\mathcal{W}|$ during a typical tap in order to be comparable to $\boldsymbol{c}, \boldsymbol{k}$ as the estimates are sums and not averages of the real parameters. There are many parameters that can be tuned in the simulations, and various estimation methods to choose amongst. The effort in this regard has been limited and considerable improvements are expected in future work.

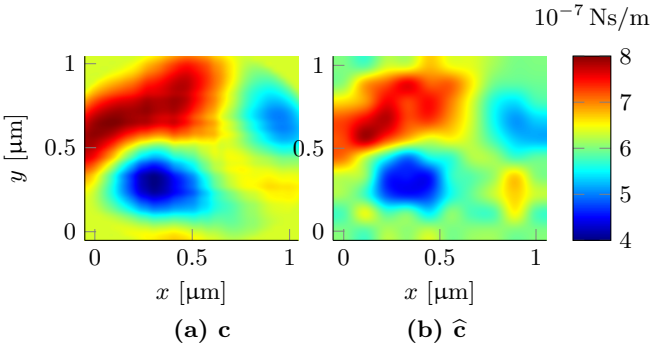

(a) c **(b) $\widehat{\mathbf{c}}$**

Fig. 4. Damping parameters mapped to the spatial domain. **(a)** Simulated damping constants, grid of 32×32. **(b)** Identified damping constants by the parameter identification scheme, grid of 10×10. The original low-resolution bitmap images have been smoothly upscaled for easier comparison.

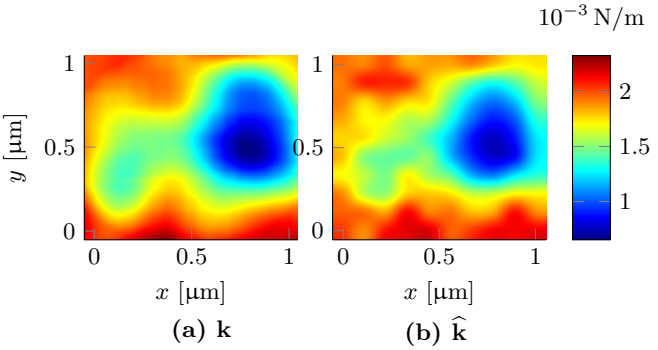

(a) k **(b) $\widehat{\mathbf{k}}$**

Fig. 5. Spring constant parameters mapped to the spatial domain. **(a)** Simulated spring constants, grid of 32×32. **(b)** Identified spring constants by the parameter identification scheme, grid of 10×10. The original low-resolution bitmap images have been smoothly upscaled for easier comparison.

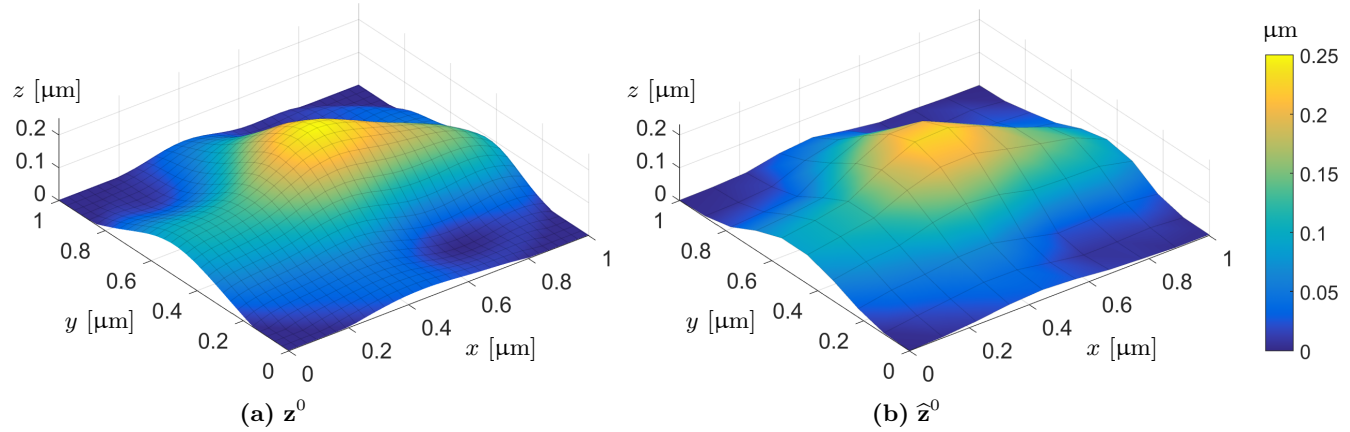

Fig. 6. Topography parameters mapped to the spatial domain. **(a)** Simulated topography. **(b)** Identified 10×10 grid of topography.

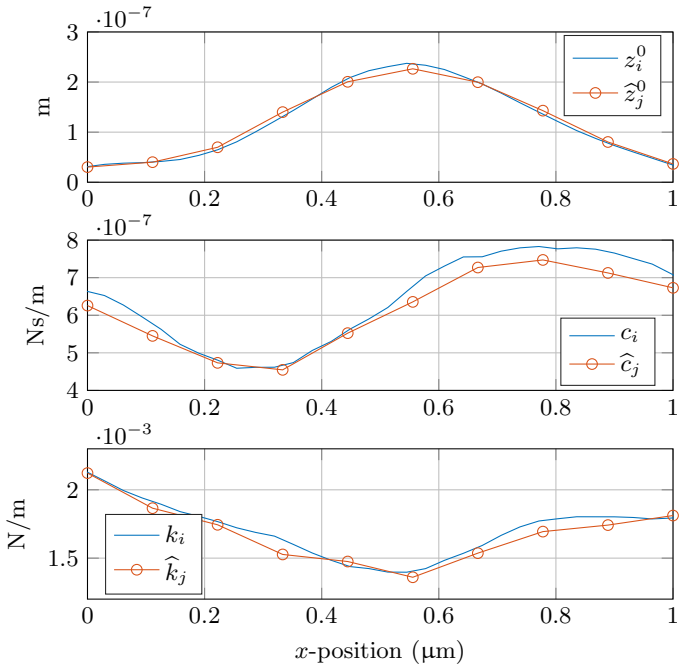

Fig. 7. Simulated parameters plotted against identified parameters along a cross section of the map at $y = 0.44\,\mu\text{m}$.

5. DISCUSSION

There is a small bias that can be seen in the estimates. This is expected in some situations. Consider a case where the cantilever performs a tap at the highest point of the sample. The described estimation method for z^0 will then identify the very tallest point. However, the surrounding area is lower than this, thus the spring force from these areas will also be lower. This will bias the spring constant towards a lower value. Equivalently, tapping at the lowest point of the sample will provide a spring constant bias in the positive direction. A smaller tip radius and lower topography gradients will improve this situation.

As remarked in the introduction, a large part of existing literature is based on static contact theory for measuring the elastic modulus of the sample, such has Hertz contact models. This theory is based on several assumptions such as small strains (indentations), homogenous sample elasticity, and frictionless surfaces (Johnson, 1985; Sokolov

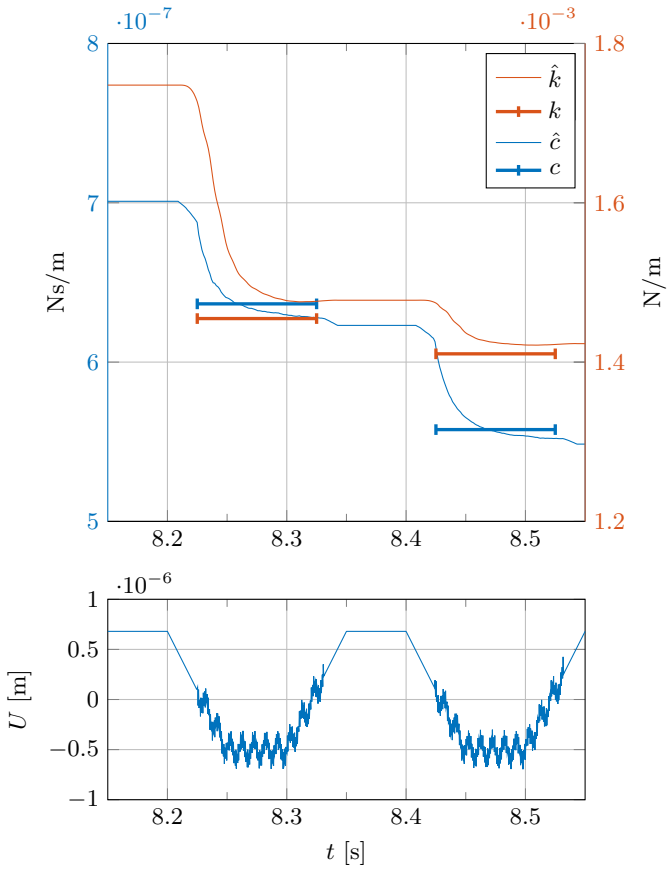

Fig. 8. Parameter identification estimates $\hat{c}, \hat{k}$, and the controlled cantilever position input U plotted over time during two taps into the sample. *Operation procedure during tap*: At $t = 8.20\,\text{s}$ the tip is lowered, at $t \approx 8.22\,\text{s}$ contact is established and parameter identification starts. At $t = 8.25\,\text{s}$ lowering stops and the cantilever is oscillated to provide a persistently exciting signal. At $t = 8.30\,\text{s}$ the parameters $\hat{c}, \hat{k}$ are recorded for the current tap j producing $\hat{c}_j, \hat{k}_j$ at the current xy-position of the cantilever, before the cantilever is raised. At $t = 8.35\,\text{s}$ the cantilever has been raised and starts moving in xy-direction. At $t = 8.40\,\text{s}$ the procedure is repeated for the next tap.

et al., 2013). The model presented in this paper however is not restricted by these limitations, or easily extendable to account for them.

- Longer indentation ranges can be accounted for by introducing nonlinear springs.
- The presented model allows for local variations in the elasticity at any spatial resolution. Identification can possibly provide estimates for spatial resolutions higher than that of the number of taps, as discussed in Section 3.
- Friction can easily be added to the model by forces.

In static Hertzian contact mechanics identifying dynamic phenomena such as damping is not possible or relevant. Since our presented model is dynamic in nature, such phenomena appear effortlessly in the model. Other dynamic phenomena can also be included in the model such as plasticity and hysteresis (Stakvik et al., 2015). However, this will require some additional effort for identifying the relevant parameters.

In contact models based on traditional Hertz theory the elastic modulus E is correlated to the indentation depth $\bar{z}$ by $E \propto \bar{z}^{1.5}$ for a spherical indenter, with experiments reporting exponents typically between 1.5 and 2.0 depending on the bluntness of the tip (Carl and Schillers, 2008). During an indentation in the simulations presented in this paper, a model fit $E = a\bar{z}^b$ for a, b, gives the exponent $b = 1.59$ as seen in Figure 9. Thus, the presented model seems to fit well with previous experiments.

Some issues may arise during future experiments. In the experiment, there may not be a clear point for which the edge of the cell is located, i.e. z^0 may not be clearly defined. This issue may be reinforced by attractive and nonlinear tip-sample forces complicating the procedure as the tip is lowered onto the sample.

The probe tip is assumed to be completely submerged into the cell during the tap. If the radius of the probe tip is very large, this may induce large stresses in the sample and the cell may permanently deform. The presented method is expected to work with only partly submerged probe tip, although the data may be skewed by the geometric nonlinearity of the probe tip. The key here is to be consistent in how the measurement is done throughout the sample. Although this may lead to bias in the identified parameters, it still allows the spatial variations of the parameters to be resolved.

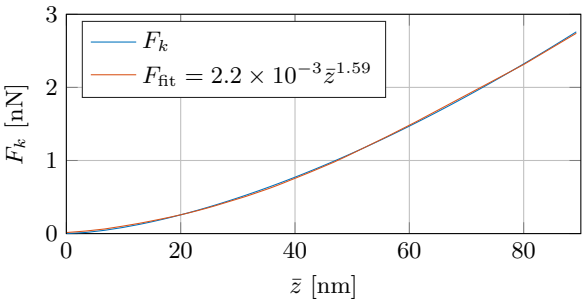

Fig. 9. Spring force F_k plotted against indentation depth $\bar{z}$. Fitting the data to the model $F_{\text{fit}} = a\bar{z}^b$ results in the exponent $b = 1.59$ which fits well with previous experimental observations.

6. FUTURE WORK

Several future extensions to the model have been discussed throughout the paper. By future experimental validations the model can easily be extended to describe additional phenomena and improved iteratively.

Additionally, in future work the topography estimate can be included in the parameter estimation directly. This will possibly reduce the estimation bias discussed earlier. However, a bilinear estimation method is then required which will somewhat increase the complexity of the estimator.

The primary reason for doing one tap at a time is to avoid frictional forces that may arise while scanning in the lateral directions with the tip still in contact with the sample. If these forces are small, the methodology presented here can be extended to in-contact dynamic mode scanning such as the approaches used in Radmacher et al. (1993); Raman et al. (2011); Cartagena-Rivera et al. (2015).

7. CONCLUSIONS

With development of new and simple techniques for parameter identification of mechanical systems, employing dynamic approaches revealing additional details of the sample's mechanical properties can become commonplace. Such approaches hold great promise for use as part of a medical diagnostic tool. This paper presents a novel approach for identifying such properties.

A dynamic model for cell mechanics is presented based on a laterally spaced grid of spring-damper elements coupled with the AFM cantilever dynamics. The model is designed to be suitable for parameter identification, and is generally applicable for any viscoelastic sample suitable for use in AFM. The parameter identification scheme is designed to identify the elastic (spring) and viscous (damping) parameters of the model. One such pair of parameters are identified at each point the cantilever taps into the sample. The parameters are guaranteed to converge exponentially fast to the real parameters by using the vertical position control signal provided in Theorem 1.

REFERENCES

Bao, G. and Suresh, S. (2003). Cell and molecular mechanics of biological materials. *Nat. Mater.*, 2(11), 715–725.

Bausch, A.R., Ziemann, F., Boulbitch, A.A., Jacobson, K., and Sackman, E. (1998). Local measurements of viscoelastic parameters of adherent cell surfaces by magnetic bead microrheometry. *Biophysics*, 75(4), 2038–2049.

Benitez, R. and Toca-Herrera, J. (2014). Looking at Cell Mechanics with Atomic Force Microscopy: Experimental and Theory. *Microscopy Research and Technique*, 77(11), 947–958.

Bhushan, B. and Marti, O. (2010). Scanning Probe Microscopy - Principle of Operation, Instrumentation, and Probes. In B. Bhushan (ed.), *Springer Handbook of Nanotechnology*, 573–617. Springer Berlin Heidelberg.

Carl, P. and Schillers, H. (2008). Elasticity measurement of living cells with an atomic force microscope: Data acquisition and processing. *Pflugers Archiv European Journal of Physiology*, 457(2), 551–559.

Cartagena-Rivera, A.X., Wang, W.H., Geahlen, R.L., and Raman, A. (2015). Fast, multi-frequency, and quantitative nanomechanical mapping of live cells using the atomic force microscope. *Scientific Reports*, 5, 11692.

Degertekin, F.L., Hadimioglou, B., Sulchek, T., and Quate, C.F. (2001). Actuation and characterization of atomic force microscope cantilevers in fluids by acoustic radiation pressure. *Applied Physic Letters*, 78(11), 1628–1630.

Discher, D.E., Boal, D.H., and Boey, S.K. (2008). Simulations of the erythrocyte cytoskeleton at large deformation. II. Micropipette aspiration. *Biophysics*, 75(3), 1584–1597.

Eielsen, A.A., Vagia, M., Gravdahl, J.T., and Pettersen, K.Y. (2013). Damping and Tracking Control Schemes for Nanopositioning. *Mechatronics, IEEE/ASME Transactions on*, 19(2), 432–444.

Garcia, R. and Perez, R. (2002). Dynamic atomic force microscopy methods. *Surface science reports*, 47(6-8), 197–301.

Guck, J., Ananthakrishnan, R., Cuningham, C.C., and Kas, J. (2002). Stretching biological cells with light. *Journal of Physics: Condensed Matter*, 14(19), 4843–4856.

Guz, N., Dokukin, M., Kalaparthi, V., and Sokolov, I. (2014). If cell mechanics can be described by elastic Modulus: Study of Different Models and Probes Used in Indentation Experiments. *Biophysical Journal*, 107(3), 564–575.

Hecht, F.M., Rheinlaender, J., Schierbaum, N., Goldmann, W.H., Fabry, B., and Schaffer, T.E. (2015). Imaging viscoelastic properties of live cells by AFM: power law rheology on the nanoscale. *Soft matter*, 11(23), 4553–4732.

Ioannou, P.A. and Sun, J. (1996). *Robust adaptive control*. Prentice Hall, Upper Saddle River, NJ.

Jeong, Y., Jayanth, G.R., Jhiang, S.M., and Menq, C.H. (2006). Direct tip-sample interaction force control for the dynamic mode atomic force microscopy. *Applied Physics Letters*, 88(20), 204102.

Johnson, K.L. (1985). *Contact mechanics*. Cambridge University Press, Cambridge.

Karvinen, K.S., Ruppert, M.G., Mahata, K., and Moheimani, S.O.R. (2014). Direct Tip-Sample Force Estimation for High-Speed Dynamic Mode Atomic Force Microscopy. *IEEE Transactions on Nanotechnology*, 13(6), 1257–1265.

Kumar, S. and Weaver, V.M. (2009). Mechanics, malignancy, and metastasis: the force journey of a tumor cell. *Cancer and Metastasis Review*, 28(1-2), 113–127.

Lekka, M., Gil, D., Pogoda, K., Dulinska-Liewka, J., Jach, R., Gostek, J., Klymenko, O., Prauzner-Bechicki, S., Stachura, Z., Wiltowska-Zuber, J., Okon, K., and Laidler, P. (2012a). Cancer cell detection in tissue sections using AFM. *Archives of Biochemistry and Biophysics*, 518(2), 151–156.

Lekka, M., Pogoda, K., Gostek, J., Klymenko, O., Prauzner-Bechicki, S., Wiltowska-Zuber, J., Jaczewska, J., Lekki, J., and Stachura, Z. (2012b). Cancer cell recognition – Mechanical phenotype. *Micron*, 43(12), 1259–1266.

Parsons, J.T., Horwitz, A.R., and Schartz, M.A. (2010). Cell adhesion: integrating cytoskeletal dynamics and cellular tension. *Nat. Review of Cellular Biology*, 11(9), 633–643.

Radmacher, M., Tillmann, R.W., and Gaub, H.E. (1993). Imaging viscoelasticity by force modulation with the atomic force microscope. *Biophysical journal*, 64(3), 735–742.

Ragazzon, M.R.P., Gravdahl, J.T., and Fleming, A.J. (2016). On Amplitude Estimation for High-Speed Atomic Force Microscopy. In *American Control Conference*. Boston, USA.

Ragazzon, M.R.P., Gravdahl, J.T., Pettersen, K.Y., and Eielsen, A.A. (2015). Topography and force imaging in atomic force microscopy by state and parameter estimation. In *American Control Conference*, 3496–3502. Chicago, USA.

Raman, A., Trigueros, S., Cartagena, A., Stevenson, A.P.Z., Susilo, M., Nauman, E., and Contera, S.A. (2011). Mapping nanomechanical properties of live cells using multi-harmonic atomic force microscopy. *Nature nanotechnology*, 6(12), 809–14.

Ramis-Conde, I., Drasdo, D., Anderson, A.R.A., and Chaplain, M.A.J. (2008). Modelling the influence of the E-Cadherin--Catenin pathway in cancer cell invasion and tissue architecture: a multi-scale approach. *Biophysics*, 95, 155–165.

Reichl, E.M., Effler, J.C., and Robinson, D.N. (2005). The stress and strain of cytokinesis. *Trends Cells Biology*, 15(4), 200–206.

Sokolov, I. (2007). Atomic Force Microscopy in Cancer Cell Research. *Cancer Nanotechnology*, 1, 1–17.

Sokolov, I., Dokukin, M.E., and Guz, N.V. (2013). Method for quantitative measurements of the elastic modulus of biological cells in AFM indentation experiments. *Methods*, 60(2), 202–213.

Stakvik, J.Å., Ragazzon, M.R.P., Eielsen, A.A., and Gravdahl, J.T. (2015). On Implementation of the Preisach Model: Identification and Inversion for Hysteresis Compensation. *Modeling, Identification and Control*, 36(3), 133–142.

Weisenhorn, A.L., Khorshandi, M., Kasas, S., Gotzos, V., and Butt, H.J. (1993). Deformation and height anomaly of soft surfaces studied with an AFM. *Nanotechnology*, 4(2), 106.